machines

MDPI

Article

Leakage Characteristics and Flow Field Regulation Mechanism of Annular Clearance Sealed Aerostatic Bearings with Conical Straight Teeth on Stator

Fusheng Wang [1] and Yongliang Wang [2,*]

[1] Marine Engineering College, Dalian Maritime University, Dalian 116026, China; 18642800705@163.com
[2] Naval Architecture and Ocean Engineering College, Dalian Maritime University, Dalian 116026, China
* Correspondence: wangyl@dlmu.edu.cn

Abstract

To address the issues of sealing leakage and airflow-induced vibration in high-speed turbomachinery, a conical straight-tooth annular clearance sealed hybrid aerostatic/aerodynamic bearing is investigated. A three-dimensional CFD model is established to study the effects of radial clearance height, inlet pressure, rotor speed, and eccentricity on pressure distribution, velocity distribution, and leakage rate. The results show that leakage exhibits a strong positive nonlinear correlation with clearance height and inlet pressure, following a power-law or polynomial relationship, while rotor speed and eccentricity exert negligible effects (less than 5%). The underlying mechanisms are identified as the kinetic energy diversion caused by circumferential shear and the mutual cancelation of throttling and backflow effects. Increasing the gap height enhances leakage by expanding the hydraulic diameter and strengthening vortex disturbance; increasing inlet pressure promotes leakage by elevating the driving force and intensifying local flow separation.

Keywords: hybrid aerostatic/aerodynamic bearing; annular clearance seal; leakage characteristics; computational fluid dynamics; flow field regulation

1. Introduction

Air bearings, with their outstanding features such as non-contact friction, zero wear, ultra-high rotational accuracy and oil-free clean lubrication, have been widely applied in high-end turbomachinery such as aero engines, steam turbines and centrifugal compressors, and are core fundamental components for ensuring the high-speed and stable operation of rotor systems. In key fields such as aerospace and energy power, turbomachinery is developing towards higher rotational speeds, higher efficiency and more severe operating conditions, which puts forward more stringent requirements for the sealing performance and operational stability of air bearings. A slight increase in sealing leakage will directly lead to a decrease in equipment efficiency, while rotor instability caused by airflow excitation may result in serious mechanical failures. Therefore, optimizing the sealing characteristics of air bearings, thus suppressing leakage and vibration risks, has become a key breakthrough for enhancing the overall performance and reliability of turbomachinery [1].

When the rotor is in a high-speed rotating state, eccentric distortion is inevitable, which causes the distribution of the circumferential pressure field in the sealing chamber to become unstable. Dominated by the fluid dynamic pressure effect, a low-pressure area

Check for updates

Academic Editor: Davide Lengani

Received: 21 March 2026
Revised: 21 April 2026
Accepted: 24 April 2026
Published: 30 April 2026

Copyright: © 2026 by the authors. Licensee MDPI, Basel, Switzerland. This article is an open access article distributed under the terms and conditions of the Creative Commons Attribution (CC BY) license.

forms in the large gap area of the seal, and a high-pressure area forms in the small gap area. Thus, a radial sealing airflow force pointing from the small gap to the large gap is generated. This force can adaptively correct the rotor eccentricity and thereby improve the dynamic stability and operational reliability of the rotor system [2]. However, under high-speed and high-pressure difference conditions, the traditional sealing structure is prone to severe airflow excitation due to the excessive fluid dynamic pressure effect, and the existence of the sealing gap inevitably leads to the leakage of the working medium, resulting in energy loss and efficiency reduction. Relevant studies have shown that the sealing leakage loss of turbine machinery accounts for 15% to 30% of the total energy loss, and airflow excitation is one of the main causes of rotor system instability, seriously restricting the upgrading of equipment to higher parameters [3].

The annular clearance seal with conical straight teeth on the stator, as a classic sealing form for hybrid aerostatic/aerodynamic bearings in turbomachinery, reduces the fluid dynamic pressure effect through the tooth-shaped throttling effect and suppresses the aerodynamic excitation force. It demonstrates significant advantages in balancing sealing stability and leakage control, and has become an important technical path for solving sealing problems in high-parameter turbomachinery [4]. However, current research on the annular clearance seal hybrid aerostatic/aerodynamic bearings with conical straight teeth on the stator still has deficiencies. The existing achievements mostly focus on the macroscopic influence of parameters such as misalignment rate and pressure ratio, but do not sufficiently explore the intrinsic mechanism of regulating leakage characteristics through core structural and operating condition parameters such as gap height and inlet pressure. There is a lack of systematic research on the coupling effect of multiple parameters and no clear engineering optimization design criteria have been formed, making it difficult to directly guide the actual product development. Therefore, conducting parametric research on the leakage characteristics of annular clearance seal hybrid aerostatic/aerodynamic bearings, revealing the regulatory laws and mechanical mechanisms of key parameters on sealing performance, and proposing scientific and reasonable parameter optimization intervals has significant theoretical value and engineering practical significance.

Regarding the dynamic characteristics and operational stability of hybrid aerostatic/aerodynamic bearings, numerous systematic studies have been conducted by scholars both at home and abroad. Chen et al. [5] constructed simulation models for different geometric configurations of groove-type air static pressure bearings and, based on the computational fluid dynamics method, analyzed the pressure distribution, bearing capacity, stiffness characteristics, and flow patterns of the bearing gap flow field, revealing the regulatory mechanism of the groove structure parameters on the static and dynamic performance of the bearings. In their research on the intake throttling compensation system, Song et al. [6] identified the correlation between the diameter of the supply air hole and the fatigue life of the bearing and, through performance testing of embedded gas bearings under variable operating conditions, quantified the coupling relationship between pressure, bearing capacity, and mass flow rate. Morosi et al. [7] developed an active aerodynamic–aerodynamic force hybrid aerostatic/aerodynamic bearing equipped with an electronic radial air injection system for high-speed flexible rotor systems. Through experiments, they verified its effective suppression of synchronous vibration and rotational instability, providing a new path to break through the performance limitations of traditional passive bearings. Radil et al. [8] systematically investigated the influence of radial clearance on the bearing load coefficient of the wing plate air bearing through load capacity tests and clarified the critical clearance interval that optimizes the bearing performance, providing a key empirical basis for the design of structural parameters of hybrid aerostatic/aerodynamic bearings. Yue Youfei et al. [9] coupled the initial structural parameters

of the hybrid aerostatic/aerodynamic bearing and established a finite element analysis model based on ANSYS. Using the response surface optimization method, they optimized the layout of the throttling holes for multiple objectives; obtained the optimal matching relationship between bearing capacity, gas consumption, and bending resistance; and completed the structural optimization design of the new hydrodynamic frictionless cylinder. Han Dongjiang et al. [10] addressed the low-frequency vibration instability problem of the high-speed gas lubrication bearing–rotor system, considering the coupling effect of gas film pressure and elastic supports. They conducted experimental research on the low-frequency vibration characteristics and, through modal analysis of the shaft system, they obtained the natural frequencies of the rotor under different supply pressure conditions. Combined with nonlinear dynamic analysis methods, they analyzed nonlinear characteristics such as the three-dimensional spectrum of frequency coupling, bifurcation diagram, and frequency spectrum after suppressing the low-frequency vibration, and proposed an optimization scheme for silicone rubber pad damping, achieving a reduction in the amplitude of the rotor's critical speed and the delay triggering of low-frequency oscillation.

In the field of research on the sealing characteristics of hybrid aerostatic/aerodynamic bearings, San Andres et al. [11] systematically reviewed experimental results and theoretical models of annular gap gas seals published since the 21st century, clarified the prediction methods and physical mechanisms of leakage volume and dynamic characteristic coefficients, and determined the regulatory laws of stiffness and damping coefficients on the stability of the rotor system. In this way, they established a comprehensive theoretical framework for the design and performance evaluation of sealing structures. Sun Dan et al. [12,13] proposed a negative misalignment sealing structure, providing a CFD methodology reference for the flow field analysis and characteristic optimization of annular clearance seals. In existing studies, for annular clearance seals with stator teeth, scholars have mostly used CFD technology to analyze the correlation between the flow field distribution and sealing performance; compared and analyzed the differences in circumferential pressure distribution between the two sealing forms; identified the influence laws of parameters such as misalignment rate, rotational speed, eccentricity, and pressure ratio on the sealing airflow force; and verified the inhibitory effect of negative misalignment seals on the fluid dynamic pressure effect and the attenuation effect on the sealing airflow excitation force. On this basis, the team combined transient flow field CFD dynamic mesh technology to establish a static and dynamic characteristic solution model for negative misalignment sealing; systematically analyzed the influence of eccentricity rate and misalignment rate on the leakage volume, circumferential pressure, airflow force, and dynamic characteristic coefficient of the sealing; and experimentally confirmed that this sealing structure can effectively reduce the sealing cross stiffness, improve the main damping, achieve the coordinated improvement of equivalent stiffness and equivalent damping, and significantly improve the operational stability of the sealing rotor system. With the development of CFD technology, CFD numerical methods have been applied to obtain static and dynamic sealing solutions. Hirano et al. [14], considering labyrinth seals, used commercial CFD programs to solve three-dimensional labyrinth seal models with eccentric rotors, compared and analyzed the differences in leakage flow and rotor dynamic sub-system predictions between CFX TASCFlow and existing body flow programs, pointed out the conservatism of body flow programs in predicting unstable forces, and provided important methodological references for the rotor dynamics analysis of rotating machinery seals. In addition, for supercritical CO_2 turbomachinery, Li Z et al. [15] used transient CFD perturbation methods to evaluate the leakage and rotor dynamic performance of three annular gas seals, and verified the inhibitory effect of the intake swirl brake on the pre-swirl and effective damping crossover frequency, providing targeted references for sealing design under high-pressure conditions.

Li P et al. [16], based on the Reynolds averaged Navier–Stokes equations and k-ω SST turbulence model, studied the axial clearance effect of the top seal of the steam turbine, revealed the regulatory mechanism of axial clearance variation on the vortex structure and leakage rate in the sealing cavity, providing experimental and numerical evidence for optimization of the leakage loss prediction model.

This study focuses on the negative misalignment structure of the conical straight-tooth hybrid aerostatic/aerodynamic bearing. The geometric structure consists of a conical straight-tooth stator and a smooth conical rotor, and the corresponding three-dimensional fluid domain model is shown in Figure 1. Compared with conventional labyrinth seals, honeycomb seals, and pocket damper seals, the conical straight-tooth structure presents better throttling effect, lower leakage loss, and more stable dynamic characteristics. A single-factor parametric analysis is performed under unified benchmark conditions to quantify the effects of clearance height, inlet pressure, rotor speed, and eccentricity. The corresponding flow mechanism is revealed, and the optimal parameter ranges are given for engineering design. Compared with conventional annular seal studies, this work provides more targeted and quantitative conclusions for high-speed rotating conditions.

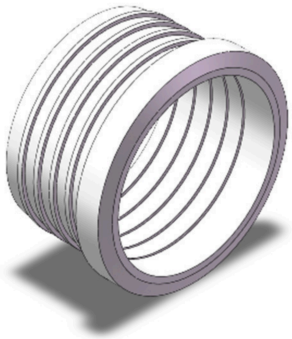

Figure 1. Fluid domain model of the air bearing mechanism.

2. Sealed Dynamic Characteristic Digital Simulation Model

2.1. Solution Model and Model Validation

To verify the accuracy and reliability of the numerical method, the labyrinth seal model reported by Hirano et al. [14] was adopted as the benchmark model. This benchmark model adopts a three-dimensional CFD method based on a rotating coordinate system to obtain the leakage flow rate and rotordynamic coefficients, which has been widely recognized in the field of seal fluid dynamics. The geometric structure consists of a smooth rotor surface and a stator with five uniformly arranged conical straight teeth, which is highly consistent with the conical straight-tooth seal structure studied in this paper. The geometric dimensions of the benchmark model are shown in Figure 2 (unit: mm). The numerical settings in the validation process are completely consistent with those in the literature, including inlet pressure, outlet pressure, rotational speed, fluid properties, and turbulence conditions. The leakage rate and dynamic stiffness coefficients obtained with the present CFD method are compared with the experimental results of Hirano et al. [14]. The relative error δ is calculated as:

$$\delta = \frac{\left|Value_{CFD} - Value_{Exp}\right|}{Value_{Exp}} \times 100\%$$

The quantitative comparison results are listed in Table 1. It can be seen that the predicted leakage rate of the present CFD model is 1.08 kg/s, while the result of Hirano's CFD is 1.28 kg/s, with a relative error of 18.5%. For dynamic stiffness coefficients, the

present results agree well with the literature data, and the maximum relative error is less than 5%. The slight difference in leakage is mainly caused by the difference in mesh refinement and interface processing. Overall, the consistency is acceptable for engineering research, indicating that the numerical method, mesh strategy, and boundary conditions adopted in this paper are reliable and feasible. Based on the benchmark model, this study establishes a three-dimensional fluid domain model of the conical straight-tooth annular clearance sealed hybrid aerostatic/aerodynamic bearing. The stator is designed with five conical straight teeth in the circumferential direction, and the rotor surface remains smooth. The tooth throttling effect is used to weaken the fluid dynamic pressure effect and improve the sealing stability. The typical operating parameters are listed in Table 1, including rotational speed, inlet pressure, outlet pressure, temperature, sealing clearance, eccentricity, and the ideal gas assumption. The structural size and boundary conditions are consistent with the actual working conditions of high-speed turbomachinery.

Table 1. Working Condition Parameters of the Sealing Solution Model.

Parameter	Values and Details	Parameter	Values and Details
rotation rate/(r/min)	60,000	inlet pressure/(MPa)	0.3
fluid	ideal gas	outlet pressure/(MPa)	0.1
turbulence model	$k-\varepsilon$ model	eccentricity	0.5
inlet temperature/K	293	sealing clearance/(mm)	0.1

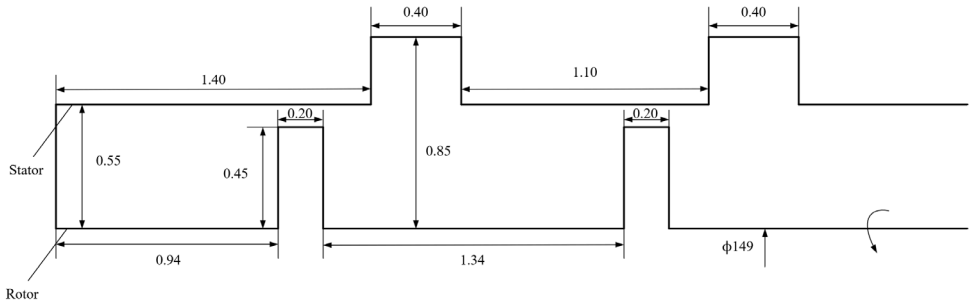

Figure 2. Geometric dimensions of the sealing model (unit: mm).

2.2. Grid Independence Verification

Regarding the flow field characteristics of the annular gap sealed hybrid aerostatic/aerodynamic bearing, the meshing process needs to give priority to capturing the fine flow in the sealing gap and representing the flow continuity of the negative misalignment surface. This is the core prerequisite for ensuring the accuracy of the calculation of radial load and leakage. As depicted in Figure 3, this study uses a structured grid to discretize the fluid domain of the bearing, implements local meshing for the core area of the sealing gap, and builds boundary layer grids that meet the requirements of the k-ε turbulence model on the rotor and stator walls. By controlling the ratio of the node spacing near the wall to ensure the accurate solution of wall shear stress and turbulence characteristics; at the same time, for the connection surface between the sealing teeth and the gap, the Interface coupling technology is adopted. By optimizing the mesh topology structure, it ensures the continuity of the pressure and velocity fields of the fluid at the tooth surface connection, avoiding numerical errors caused by mesh mismatch.

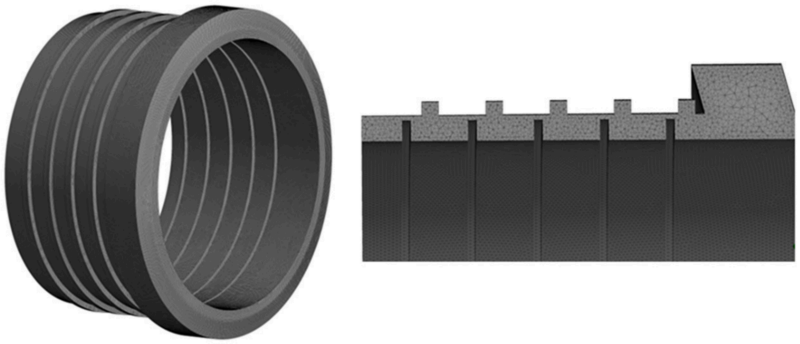

Figure 3. Model Grid Division.

To achieve grid independence verification, six sets of structured grid schemes with different numbers of grid cells were selected. The number of grid cells was set to 381,327, 606,487, 832,428, 1,182,444, 1,495,090, and 1,856,347 and the number of nodes was 85,739, 133,521, 178,789, 249,101, 314,314, and 385,297, respectively. During the verification process, the core operating parameters such as inlet and outlet pressure (0.3 MPa for inlet and 0.1 MPa for outlet) and rotor speed (60,000 r/min) were strictly maintained unchanged. The bearing radial load under each grid scheme was solved using the ANSYS CFX 2021 R1 software, and the relationship between the number of grid cells and the radial load was obtained as shown in Figure 4. Taking the radial load corresponding to the maximum number of grid cells as the benchmark, the relative deviation of the radial load in each of the other grid schemes was calculated. When the relative deviation of the radial load between two adjacent grids does not exceed 5%, it is considered that the grid number has met the independence requirement. As can be seen from Figure 4, the model obtained by grid division with 314,314 nodes and 1,495,090 grid cells met the accuracy requirements for simulation calculation, and this grid number was selected as the grid scheme for subsequent simulations. The selected grid scheme ensures reliable and consistent results for radial load, leakage rate, and pressure distribution. In addition to radial load, leakage rate and pressure distribution were also adopted to verify grid independence. All key physical quantities, including radial load, leakage rate, and pressure distribution, exhibited consistent and stable convergence trends with grid refinement. No obvious fluctuations or deviations were observed among different grid schemes, which fully ensures that the selected grid scheme is reliable, universal, and sufficiently accurate for the subsequent parametric analysis.

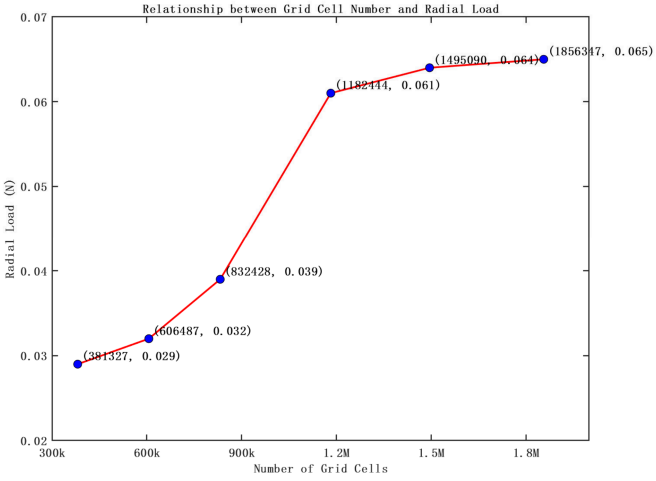

Figure 4. Radial load versus grid cell number.

2.3. Boundary Condition Setting and Numerical Methods for Solving the Model

Based on the actual working scenarios of the hybrid aerostatic/aerodynamic bearings and fluid dynamics theory, the boundary conditions for the three models were set uniformly and in accordance with the physical reality in ANSYS CFX-Pre. As illustrated in Figure 5, the fluid domain consists of the rotor, stator, inlet and outlet regions. The inlet boundary adopts the pressure inlet boundary (Total Pressure), with the inlet total pressure set to 0.3 MPa, the default temperature is 293 K, and the pre-rotation speed of the airflow is set to 0, to simulate the inflow state of the gas in the actual working condition; the outlet boundary adopts the pressure outlet boundary (Static Pressure), with the outlet static pressure set to 0.1 MPa, allowing the fluid to freely flow back, avoiding the interference of the backflow phenomenon in the outlet area on the calculation results. The rotor wall surface is set as a rotating wall (Rotating Wall), with the rotational speed consistent with the actual rotor speed (60,000 r/min), the rotation direction the same as the actual rotation direction of the rotor, the wall surface is treated as adiabatic, ignoring the influence of wall heat exchange on the fluid flow; the stator wall surface is set as a stationary wall (Stationary Wall), also using adiabatic treatment, and set as a no-slip boundary condition (No-Slip Wall), which conforms to the physical state of the stator being fixed and the fluid velocity being 0 near the wall in the actual structure. Meanwhile, the structure of this bearing has an interface connection surface between the sealing teeth and the clearance. By adopting the Interface contact surface unit boundary technology, the fluid regions of the tooth surface and the clearance are coupled and connected, ensuring the continuity of pressure and the conservation of velocity at the misaligned surface, and maintaining the integrity and continuity of the flow field.

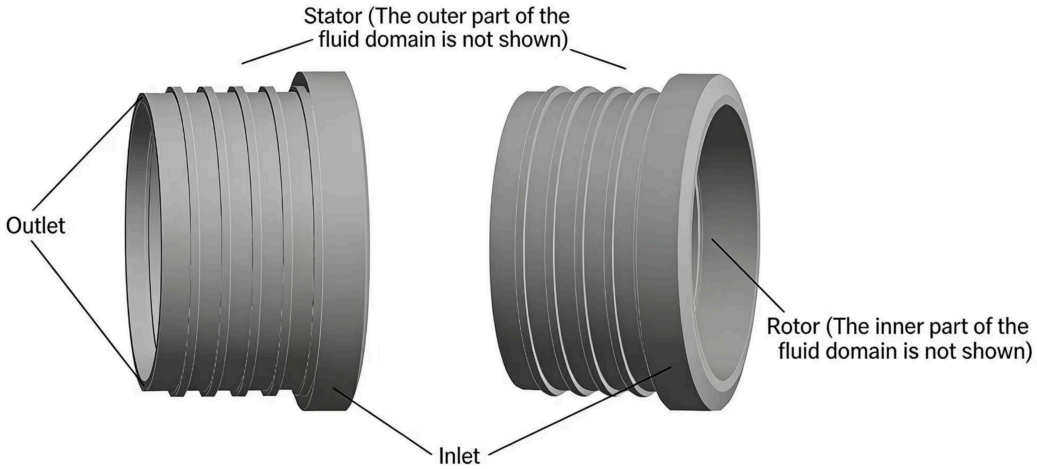

Figure 5. Introduction to the Fluid Domain Model.

The governing model adopts the k-ω SST turbulence model, which is more suitable for high-speed rotating flow in narrow annular gaps, capturing streamline curvature, rotation effects, and potential Taylor–Couette instabilities more accurately [17]. The near-wall mesh is refined to ensure $y^+ < 1$ for enhanced wall treatment. A density-based solver is adopted in the numerical solution, which is particularly suitable for transonic and highly compressible flow conditions in the sealing gap. This solver directly solves the conservation equations of mass, momentum, and energy in their conservative form, ensuring high robustness and accuracy for flows with large density variations and shock waves [18]. Compared with the pressure-based solver, the density-based scheme better captures the compressibility effect and flow field discontinuity, thereby improving the rationality of the numerical method and the reliability of the prediction results. The convergence criterion is set such that the root-mean-square (RMS) residuals of all governing equations decrease to below

10^{-6}. As illustrated in Figure 6, the residual curves decrease rapidly and stabilize within a sufficient number of iteration steps, indicating that the numerical solution reaches a stable and reliable convergence state. In this paper, the ideal gas assumption is adopted. Within the pressure range of 0.1–1.5 MPa studied, the compressibility factor Z of air is very close to 1.0, and the deviation caused by real gas effects is less than 2%, which is negligible for engineering applications. Therefore, the ideal gas model is reasonable and sufficiently accurate.

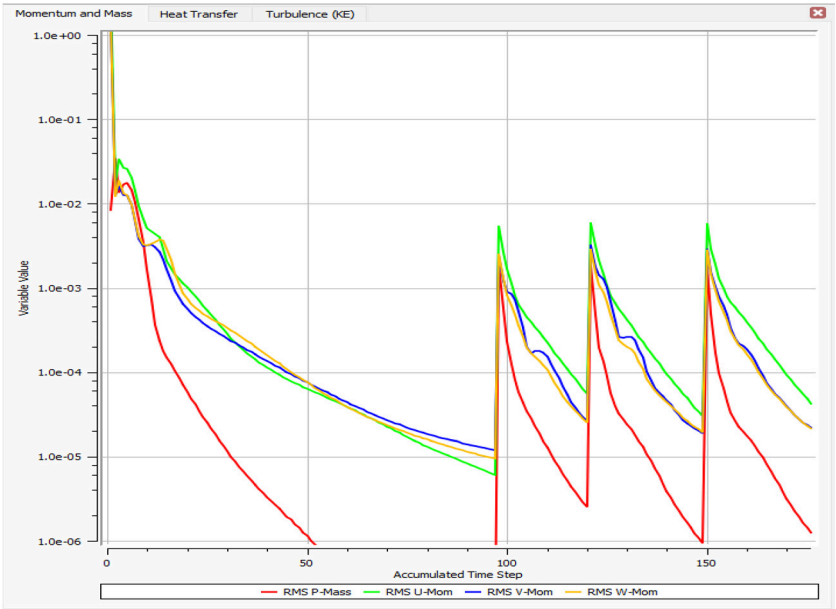

Figure 6. Convergence history of RMS residuals for the governing equations.

3. Study on Sealing Leakage Characteristics

3.1. The Influence of Clearance Height on the Leakage Characteristics of Hybrid Aerostatic Bearings

The radial clearance height of the air bearing is a core structural parameter that determines its sealing performance and leakage volume, directly affecting the operating efficiency and stability of the bearing. Its reasonable design is a key prerequisite for achieving high-precision and low-loss operation of air bearings. Based on the theory of steady compressible gas flow and using the computational fluid dynamics (CFD) numerical simulation method, with the inlet pressure of 0.3 MPa, outlet pressure of 0.1 MPa, rotor speed of 60,000 r/min, and eccentricity $\varepsilon = 0$ as the reference working condition, five groups of radial clearance heights of 0.02 mm, 0.04 mm, 0.06 mm, 0.08 mm, and 0.10 mm were set. Parameterized simulation research was carried out to systematically explore the influence laws of clearance height on the pressure distribution, velocity distribution, and leakage volume in the sealing gap; clarify the mechanism of the clearance height; and provide a reliable theoretical basis and quantitative reference for the structural optimization design of air bearings.

3.1.1. The Influence of Gap Height on the Pressure Distribution of the Gap Flow Field

Figure 7 shows the pressure distribution cloud diagram within the sealing gap of the air bearing for different gap heights.

By comparing the pressure distribution maps under different gap heights, it can be observed that as the gap height increases from 0.02 mm to 0.10 mm, the high-pressure area at the inlet significantly shrinks, while the low-pressure area expands significantly towards the inlet side. The pressure attenuation process gradually concentrates in the first 1/4 area before the seal, and the pressure loss rate significantly increases to 23.5%. The

pressure gradient shows a significant increase with the increase in gap height, and the non-uniformity of the flow field pressure distribution continues to intensify.

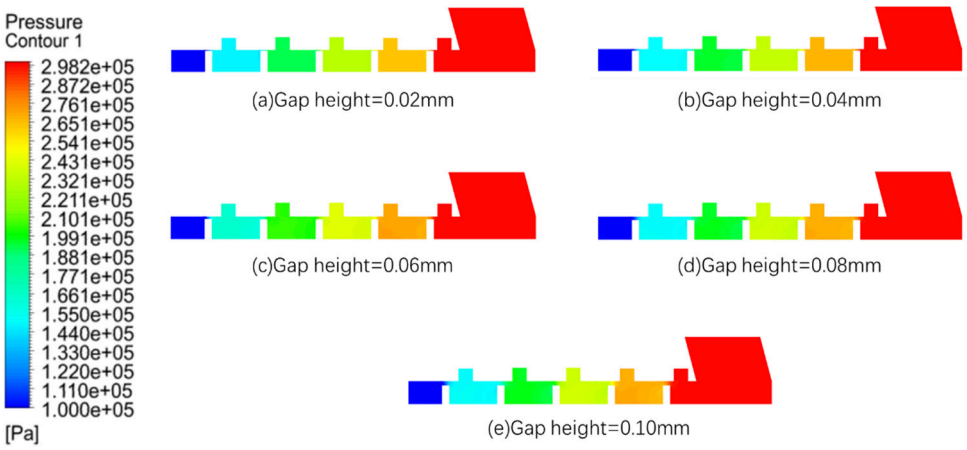

Figure 7. Pressure contour map of the gap flow field under different gap heights.

Under each gap height condition, a low-pressure vortex is formed near the sealing inlet due to the sudden change in the cross-section of the flow channel. The pressure at the center of the vortex decreases significantly with the increase in gap height; for example, the pressure at the center of the vortex in the radial gap of 0.02 mm is 0.22 MPa, and it drops to 0.15 MPa in the radial gap of 0.10 mm. At the same time, the influence range of the vortex expands with the increase in gap height. From 0.02 mm, it extends 0.5 mm along the axial direction, and expands to 1.2 mm along the axial direction in the radial gap of 0.10 mm. The disturbance effect on the pressure distribution is significantly enhanced. Due to the combined effect of gas compressibility and gravity, the asymmetry of the pressure distribution in the flow field above and below the rotor becomes more significant as the gap height increases. The maximum pressure difference between the upper and lower parts in the radial gap of 0.02 mm is 0.03 MPa, and it increases to 0.08 MPa in the radial gap of 0.10 mm. Throughout the entire sealing length range, the pressure drop rate of the lower part of the flow field is always higher than that of the upper part; this phenomenon is due to the additional influence of gravity on gas flow, and becomes more prominent as the gap height increases [19].

From the analysis of the fluid mechanics mechanism, an increase in the gap height leads to a significant expansion of the hydraulic diameter of the flow channel, a substantial reduction in the frictional resistance of the gas along the flow path, a significant improvement in the efficiency of energy conversion from pressure to kinetic energy and, consequently, a sharp increase in the pressure gradient as the gap height increases. At the same time, in the case of large gap conditions, there is ample space for gas molecule diffusion, and the disturbance effect of the inlet vortex on the pressure distribution of the main flow field is further enhanced, resulting in an exacerbation of the non-uniformity of the pressure attenuation process. Eventually, the aforementioned pressure distribution pattern is formed, which is consistent with the flow characteristics of compressible gases in narrow slit flow channels [20].

3.1.2. The Influence of Gap Height on the Velocity Distribution of the Gap Flow Field

Figure 8 shows the contour plots of the axial velocity distribution at the inlet of the sealing gap under different gap heights.

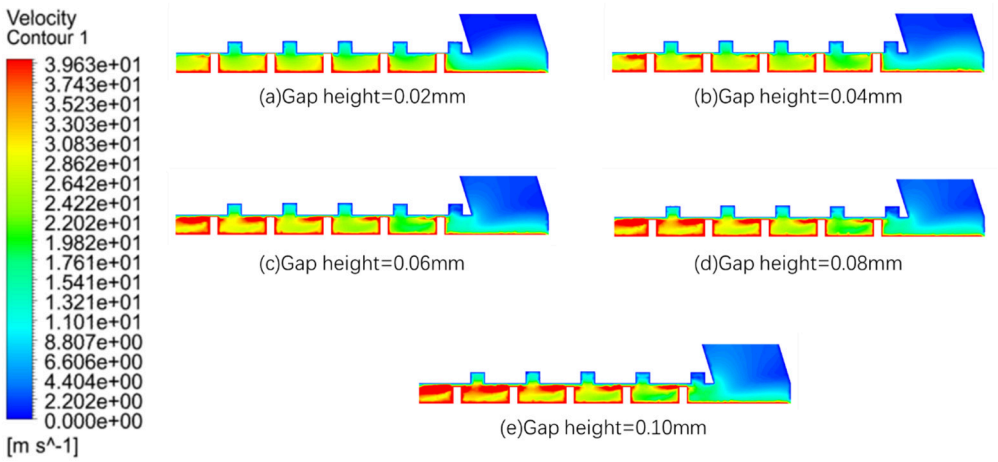

Figure 8. Axial velocity contour map of the gap flow field under different gap heights.

As shown in Figure 8, when the gap height is 0.02 mm, the axial velocity within the sealing gap is mainly at medium and low speeds, and the axial distribution uniformity is relatively high. From the inlet to the outlet, the axial velocity increase is small, and the flow field stability is good. This is mainly due to the large gas flow resistance under a small gap, and the conversion of pressure energy to kinetic energy is restricted.

As the gap height gradually increases to 0.10 mm, the axial velocity peak significantly increases, the high-speed area coverage expands, and the axial velocity along the path increases, while the velocity distribution uniformity decreases. This is because the increase in gap height directly leads to the expansion of the flow passage area, and the gas flow resistance significantly decreases. Under the constant inlet and outlet pressure difference, the efficiency of the conversion of pressure energy to kinetic energy significantly improves.

Furthermore, under the condition of a large gap, a distinct local backflow phenomenon occurs near the sealing inlet, and the backflow range gradually expands as the gap height increases. Specifically, with a gap height of 0.08 mm, the axial length of the backflow area along the axis is 0.3 mm, and with a gap height of 0.10 mm, the axial length of the backflow area along the axis increases to 0.5 mm. This phenomenon is caused by the significant enhancement of gas fluidity under large gap conditions, and the disturbance effect of the inlet vortex on the main flow field intensifies, resulting in reverse flow of gas in a local area, which in turn affects the overall stability of the flow field. This is also an important reason for the decrease in the uniformity of the velocity distribution under large gap conditions.

3.1.3. The Influence of Clearance Height on the Leakage of Hybrid Aerostatic/Aerodynamic Bearings

Table 2 presents the calculation results of the leakage volume of the hybrid aerostatic bearing seal at different gap heights. Figure 9 shows the graph of the leakage volume of the hybrid aerostatic bearing seal varying with the gap height.

Table 2. Calculation Results of Gap Leakage Volume at Different Gap Heights.

Eccentricity	Inlet Pressure (MPa)	Rotor Speed (r/min)	Gap Height (mm)	Gap Leakage Rate (kg/s)
0	0.3	60,000	0.02	0.000358
			0.04	0.000776
			0.06	0.00120
			0.08	0.00161
			0.10	0.00199

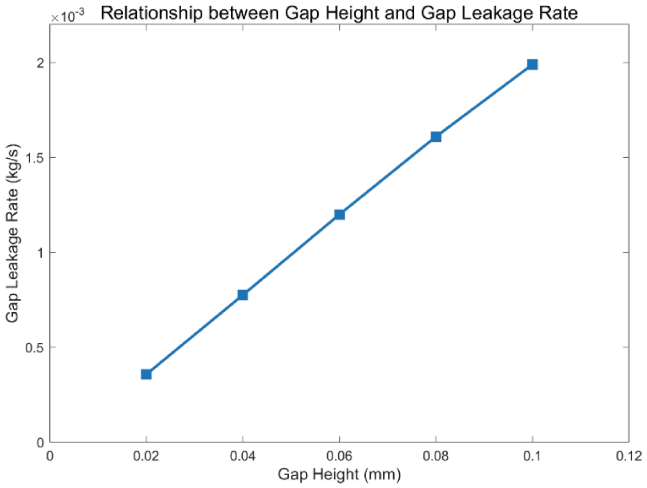

Figure 9. Variation in Gap Leakage Quantity with Gap Height.

From Table 2 and Figure 9, it can be seen that as the height of the sealing gap increases, the leakage volume of the seal increases significantly. The relationship is nonlinear, closer to a power-law or polynomial trend, with a faster growth rate at small clearances and a slower rate at large clearances. This is mainly because under the condition of a small gap, the flow passage area is smaller, and a slight change in the gap will cause significant changes in the flow passage area and flow resistance, thereby having a significant impact on the leakage volume; meanwhile, under a large gap condition, the flow passage area is already at a relatively large level, the influence of the gap change on the flow passage area and flow resistance weakens, and the increase in the leakage volume also decreases accordingly. Regression analysis with R^2 values and comparison with classical scaling laws (clearance exponent ~1.5–2.5) confirm the nonlinear nature of this relationship.

For engineering design, the clearance height should be controlled within 0.03–0.06 mm to balance leakage control and operational safety. Based on the comprehensive simulation results, the gap height should be controlled within the range of 0.03 to 0.06 mm as much as possible. This can effectively achieve the coordinated optimization of leakage volume and suspension stability, balancing the working performance and service life of the air bearing.

3.2. The Influence of Inlet Pressure on the Leakage Characteristics of Hybrid Aerostatic/Aerodynamic Bearings

The inlet pressure is one of the key parameters in the operating conditions of the hybrid aerostatic/aerodynamic bearing. Its magnitude directly determines the driving force of the gas flow, and subsequently affects the flow field distribution and leakage characteristics within the sealing gap. Based on the theory of steady compressible gas flow, under the reference operating condition of a radial clearance height of 0.10 mm, an outlet pressure of 0.1 MPa, a rotor speed of 60,000 r/min, and an eccentricity of $\varepsilon = 0$, five groups of inlet pressures of 0.3 MPa, 0.6 MPa, 0.9 MPa, 1.2 MPa, and 1.5 MPa were set. Parameterized simulation studies were conducted to systematically explore the influence laws of the inlet pressure on the pressure distribution, velocity distribution, and leakage volume within the sealing gap; clarify the mechanism of the inlet pressure; and provide theoretical support for the condition matching design of hybrid aerostatic/aerodynamic bearings.

3.2.1. The Influence of Inlet Pressure on the Pressure Distribution of the Gap Flow Field

Figure 10 shows the pressure distribution contour plot at the inlet of the sealing gap under different inlet pressures.

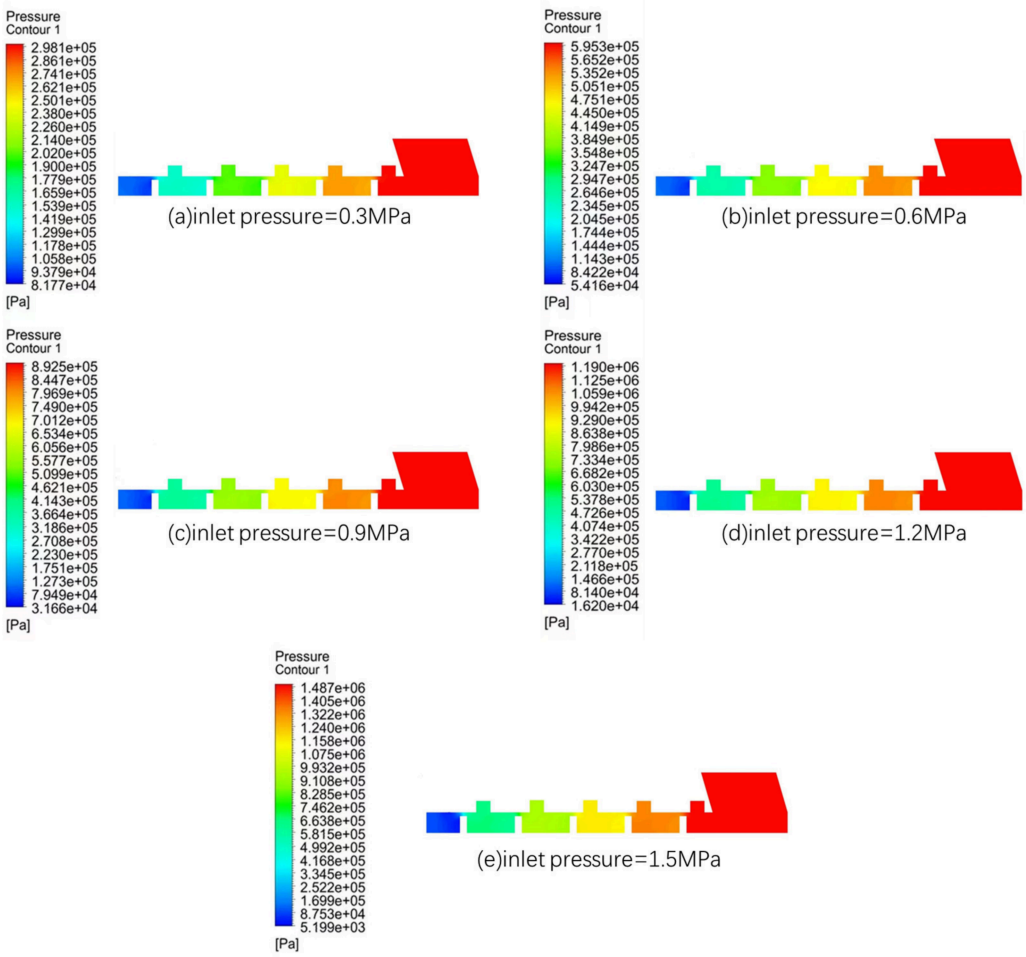

Figure 10. Pressure contour map of the gap flow field under different inlet pressures.

As shown in Figure 10, as the inlet pressure increased from 0.3 MPa to 1.5 MPa, the overall pressure level within the sealing gap significantly rose and the axial extension range of the high-pressure area continued to expand. The gradient characteristics of the pressure attenuation process became more obvious, the pressure drop rate in the inlet section accelerated, the low-pressure area migrated towards the sealing middle section, and the pressure loss rate gradually rose to 39.5%.

From the detailed characteristics of the pressure distribution, the increase in the inlet pressure strengthens the low-pressure vortex effect at the sealing inlet. When the inlet pressure is 0.3 MPa, the pressure at the center of the inlet vortex is 9.379×10^4 Pa, and the influence range of the vortex along the axial direction is approximately 0.4 mm. When the inlet pressure is 1.5 MPa, the pressure at the center of the vortex drops to 8.753×10^4 Pa, and the influence range expands to 0.7 mm. Moreover, the pressure gradient difference between the vortex area and the main flow field significantly increases. This phenomenon is due to the increase in the inlet pressure, which enhances the inertial force of the gas, and the local flow separation effect at the sudden change in the flow channel cross-section becomes more pronounced, thereby intensifying the disturbance on the pressure distribution [21].

From the perspective of fluid mechanics, the inlet pressure is the core driving force for gas flow. An increase in the inlet pressure directly enhances the pressure potential energy of the flow field, strengthening the conversion of pressure energy into kinetic energy. Therefore, the pressure gradient increases as the inlet pressure rises. At the same time, under high pressure, the compressibility characteristics of the gas become more prominent. The local structure of the flow channel, such as the inlet corner, has a more significant

obstructive effect on the flow, leading to more obvious pressure losses. Eventually, a pressure distribution pattern is formed where the overall pressure increases, the gradient becomes larger, and the vortex disturbance intensifies [22].

3.2.2. The Influence of Inlet Pressure on the Velocity Distribution of the Gap Flow Field

Figure 11 presents the contour plots of the axial velocity distribution at the inlet of the sealing gap under different inlet pressures. As can be seen from Figure 11, as the inlet pressure increases from 0.3 MPa to 1.5 MPa, the peak axial velocity continuously rises, and the coverage range of the high-speed area along the axial direction significantly expands. The high-speed zone in the inlet section extends to one-third of the sealing length, and the velocity in the middle section also rises to the range of 20–30 m/s, with the gradient characteristics of the velocity distribution becoming more obvious.

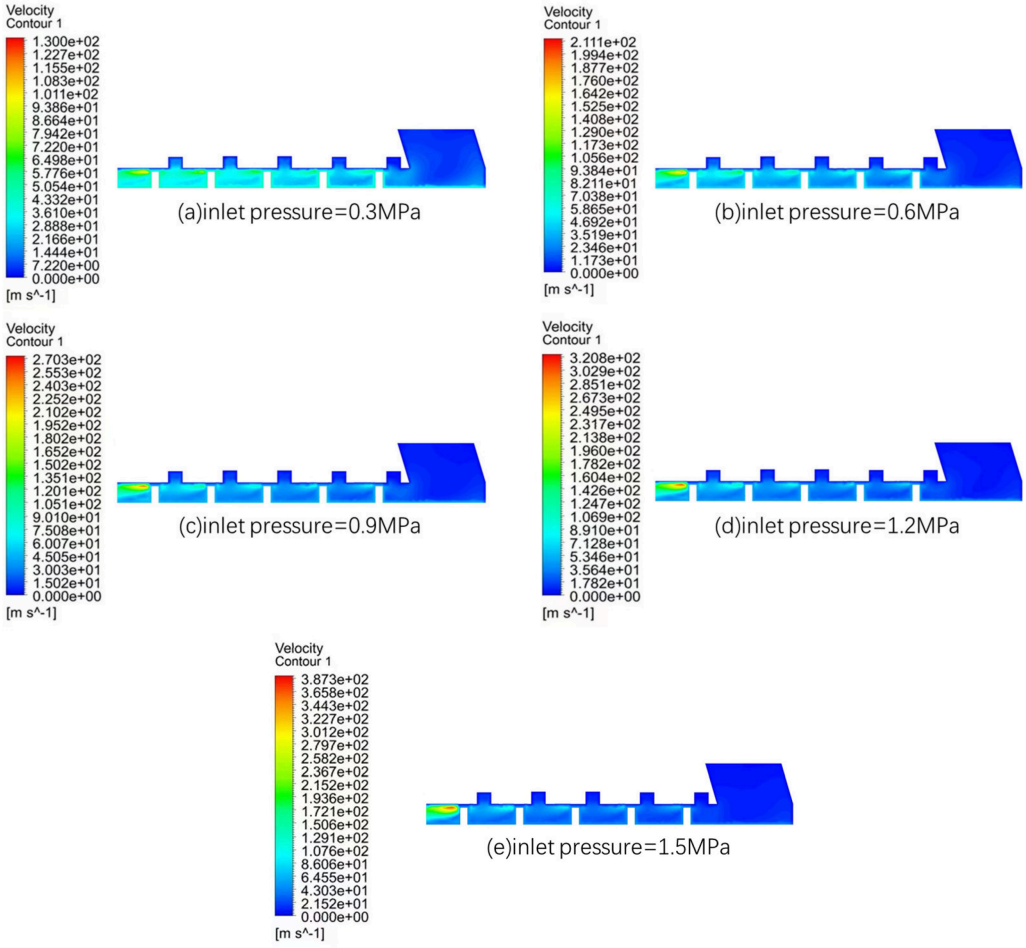

Figure 11. Axial velocity contour map of the gap flow field under different inlet pressures.

The increase in inlet pressure simultaneously intensifies the local backflow phenomenon at the sealing inlet. When the inlet pressure is 0.3 MPa, the axial length of the inlet backflow area is approximately 0.2 mm; when the inlet pressure is 1.5 MPa, the backflow area expands to 0.5 mm, and the peak backflow velocity increases from 15 m/s to 40 m/s. This phenomenon is directly related to the vortex strengthening effect after the increase in inlet pressure. The expansion of the backflow area further exacerbates the non-uniformity of the flow field, but its influence on the velocity in the main flow direction remains secondary.

3.2.3. The Influence of Inlet Pressure on the Leakage of Hybrid Aerostatic/Aerodynamic Bearings

Table 3 presents the calculation results of the leakage volume of the air-float bearing seal under different inlet pressures. Figure 12 shows the variation in the leakage volume of the air-float bearing seal with the inlet pressure.

Table 3. Calculation Results of Gap Leakage Volume under Different Inlet Pressures.

Gap Height (mm)	Eccentricity	Rotor Speed (r/min)	Inlet Pressure (MPa)	Gap Leakage Rate (kg/s)
0.1	0	60,000	0.3	0.00199
			0.6	0.00386
			0.9	0.00561
			1.2	0.00738
			1.5	0.00898

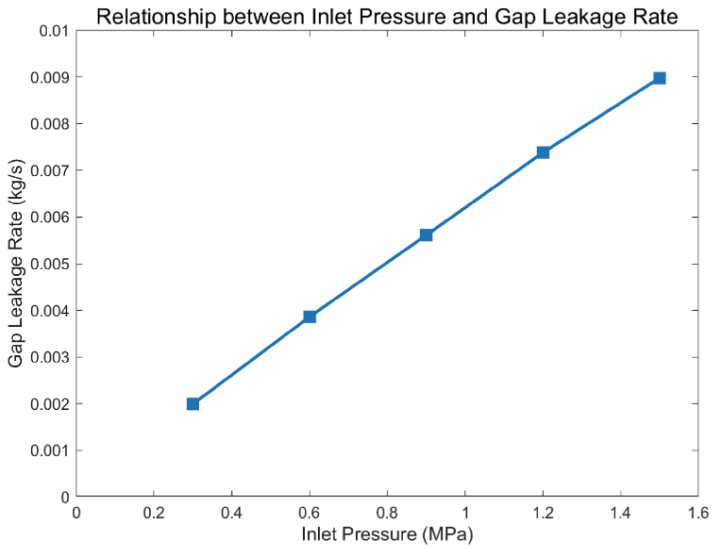

Figure 12. Variation in Gap Leakage Volume with Inlet Pressure.

From Table 3 and Figure 12, it can be seen that the gap leakage volume increases significantly with an increase in inlet pressure, showing a strong positive nonlinear relationship. The leakage growth rate gradually slows down under high pressure due to the influence of air compressibility. The increase in inlet pressure significantly increases the axial flow velocity, thereby raising the leakage rate. Meanwhile, the compressibility of air is weak in the low-pressure range, so the flow rate responds more significantly to pressure variation. In the high-pressure range, the increased compressibility causes part of the pressure energy to be consumed in gas compression, so the growth rate of axial velocity and leakage slows down, showing an obvious nonlinear trend.

3.3. The Influence of Rotor Speed on the Leakage Characteristics of Hybrid Aerostatic/Aerodynamic Bearings

The rotor speed is one of the key parameters for the operation of a hybrid aerostatic bearing. It affects the flow field distribution within the sealing gap by altering the circumferential motion state of the fluid, thereby influencing the leakage characteristics. Based on the theory of steady compressible gas flow, under the reference operating condition of a radial gap height of 0.10 mm, inlet pressure of 0.3 MPa, outlet pressure of 0.1 MPa, and eccentricity $\varepsilon = 0$, five rotor speed groups of 60,000 r/min, 80,000 r/min, 100,000 r/min, 120,000 r/min, and 140,000 r/min were set for parametric simulation research. This study systematically

explores the influence laws of rotor speed on the flow field pressure distribution, velocity distribution, and leakage volume within the sealing gap, clarifies the mechanism of rotor speed, and provides a theoretical basis for the adaptation of hybrid aerostatic bearings to high-speed operating conditions.

3.3.1. The Influence of Rotor Speed on the Pressure Distribution of the Gap Flow Field

Figure 13 presents the pressure distribution contour plot within the sealing gap of the hybrid aerostatic bearing under different rotor speeds. When the rotor speed is 60,000 r/min, the maximum pressure value in the pressure field within the sealing gap is 2.981 $\times$ 10^5 Pa. The pressure gradually decreases smoothly from the inlet to the outlet. The low-pressure area is concentrated in the sealing outlet section, and the pressure loss rate is 34.0%. As the rotor speed gradually increases to 140,000 r/min, the overall pressure distribution pattern within the sealing gap does not show significant changes, but the uniformity of pressure attenuation slightly improves: the extension range of the high-pressure area along the pipeline in the inlet section slightly expands, the gradient fluctuation of the low-pressure area in the outlet section weakens, and the pressure loss rate slowly decreases from 34.0% to 33.2%, with a relatively small change [23].

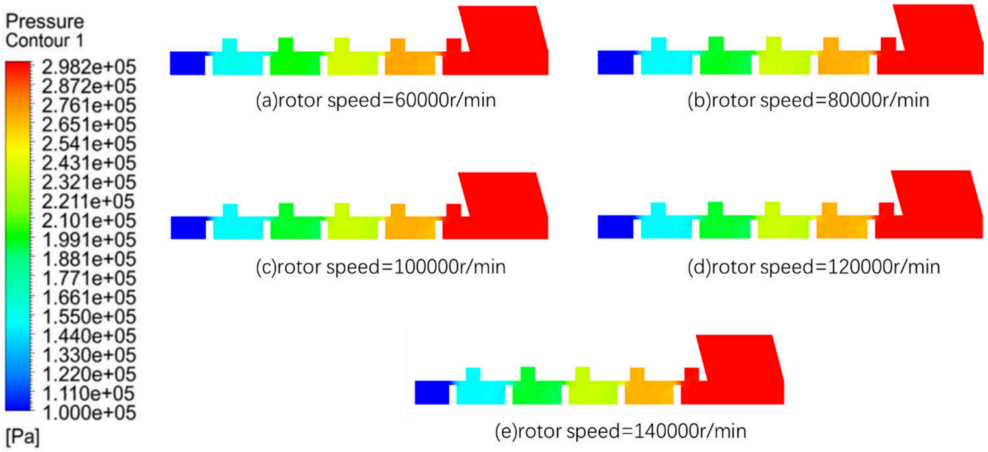

Figure 13. Pressure contour map of the gap flow field under different rotor speeds.

From the detailed characteristics of the pressure distribution, the increase in rotor speed has a relatively limited impact on the inlet low-pressure vortex. When the rotor speed is 60,000 r/min, the pressure at the center of the inlet vortex is 9.379 $\times$ 10^4 Pa and the influence range of the vortex along the axial direction is approximately 0.4 mm; when the rotor speed is 140,000 r/min, the pressure at the center of the vortex only drops to 9.216 $\times$ 10^4 Pa and the influence range expands to 0.45 mm. The difference between the two is small. This phenomenon is due to the fact that the rotor speed mainly changes the circumferential motion of the fluid, and its direct driving effect on the axial pressure gradient is weak. Therefore, the influence of the rotor speed on the pressure distribution is much lower than parameters such as the gap height and inlet pressure [24].

3.3.2. The Influence of Rotor Speed on the Velocity Distribution of the Gap Flow Field

Figure 14 clearly presents the velocity distribution contour plot within the sealing gap of the hybrid aerostatic bearing under different rotor speeds. From Figure 14, it can be seen that the high-speed area is concentrated in the sealing inlet section, and the axial extension range is relatively narrow [25].

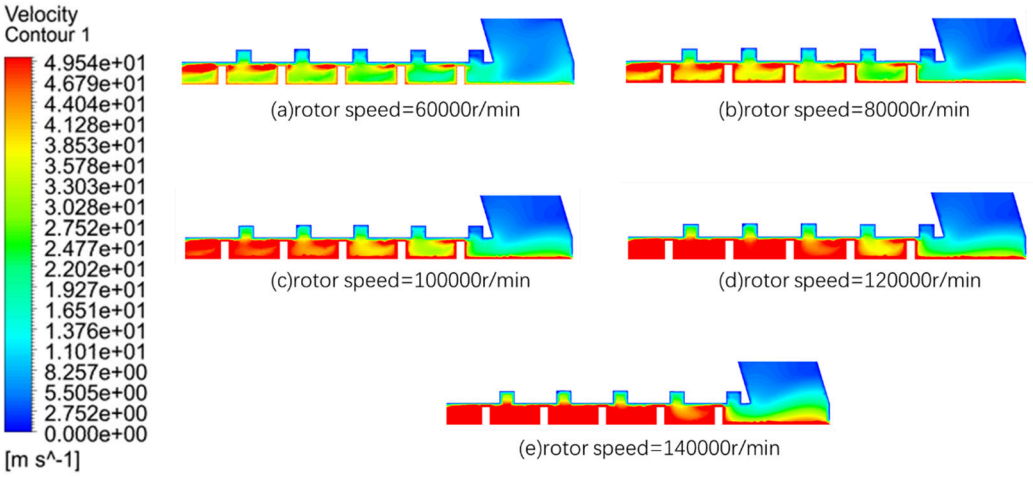

Figure 14. Axial velocity contour map of the gap flow field under different rotor speeds.

The variation in axial velocity is weakly negatively correlated with circumferential velocity. When the rotor speed is 140,000 r/min, the peak axial velocity is slightly lower compared to when the rotor speed is 60,000 r/min, with a decrease of approximately 6%. This phenomenon is due to the enhanced circumferential shear effect, which diverts part of the axial flow kinetic energy, causing the axial velocity to slightly decrease with the increase in rotor speed. However, since the driving force of axial flow (the pressure difference between the inlet and outlet) remains unchanged, the variation range of axial velocity is much smaller than that of circumferential velocity. Thus, the influence of rotor speed on the axial flow field is relatively weak [26].

3.3.3. The Influence of Rotor Speed on the Leakage of Hybrid Aerostatic/Aerodynamic Bearings

Table 4 presents the calculation results of the leakage volume of the hybrid aerostatic bearing seal under different rotor speeds. Figure 15 shows the graph of the leakage volume of the hybrid aerostatic bearing seal varying with the rotor speed.

Table 4. Calculation Results of Gap Leakage Volume at Rotational Speed of the Rotor.

Gap Height (mm)	Eccentricity	Inlet Pressure (MPa)	Rotor Speed (r/min)	Gap Leakage Rate (kg/s)
0.10	0	0.3	60,000	0.00199
			80,000	0.00197
			100,000	0.00195
			120,000	0.00193
			140,000	0.00189

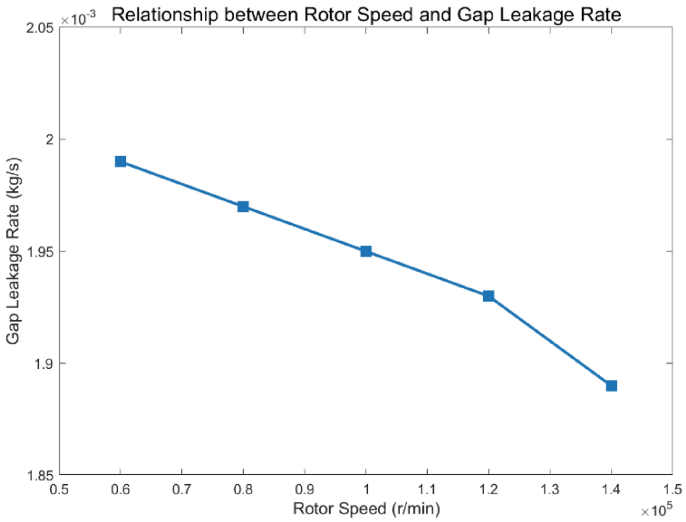

Figure 15. Variation in Gap Leakage Quantity with Rotational Speed of the Rotor.

From Table 4 and Figure 15, it can be seen that as the rotor speed increases, the gap leakage volume gradually decreases. Compared with changing the gap height, sealing length, and inlet pressure, the influence of rotor speed variation on the gap leakage volume is relatively small. This is mainly because when the rotor rotates at high speed, the gas in the gap is driven by the no-slip boundary condition on the wall to undergo intense circumferential shear motion, forming significant circumferential flow. According to the principle of momentum conservation, the total kinetic energy of the gas in the gap is composed of axial flow kinetic energy and circumferential flow kinetic energy. Under the condition of constant inlet and outlet pressure difference, the total energy input remains unchanged. As the rotor speed increases, the circumferential shear effect strengthens and more energy is distributed to the circumferential flow, resulting in the diversion of axial flow kinetic energy and a slight decrease in the peak axial velocity. Since the leakage volume is directly related to the axial velocity, the diversion of axial kinetic energy ultimately leads to a slow decrease in leakage volume with increasing rotor speed.

3.4. The Influence of Eccentricity on the Leakage Characteristics of Hybrid Aerostatic/Aerodynamic Bearings

The eccentricity is a key structural parameter that reflects the degree of concentricity between the rotor and the stator of the hybrid aerostatic bearing. It affects the flow field characteristics by altering the asymmetric distribution of the sealing gap, and subsequently influences the leakage volume. Based on the theory of steady compressible gas flow, under the reference working condition of a radial gap height of 0.10 mm, an inlet pressure of 0.3 MPa, an outlet pressure of 0.1 MPa, and a rotor speed of 60,000 r/min, five eccentricity groups of 0, 0.1, 0.3, 0.5, and 0.7 are set for parameterized simulation research. This study systematically explores the influence laws of eccentricity on the pressure distribution, velocity distribution, and leakage volume within the sealing gap, clarifies the mechanism of eccentricity, and provides theoretical support for the design of assembly accuracy and operational stability of hybrid aerostatic bearings.

3.4.1. The Influence of Eccentricity on the Pressure Distribution of the Gap Flow Field

Figure 16 presents the pressure distribution characteristics within the sealing gap of the hybrid aerostatic bearing under different eccentricities. As the eccentricity increases from 0 to 0.7, the asymmetry of the sealing gap significantly enhances, and the symmetrical form of the pressure distribution is disrupted. The pressure decay rate on the rotor's biased side accelerates, the extension range of the high-pressure area along the axial direction

shortens, and the local pressure gradient sharply increases; the pressure decay rate on the rotor's deviated side slows down, the low-pressure area expands towards the inlet side and, due to local reflux, a low-pressure vortex is formed and the non-uniformity of the pressure distribution intensifies. However, due to the mutual cancelation of the effects on both sides, the overall pressure loss rate fluctuates only from 34.0% to 33.7%, with a change range of less than 1%.

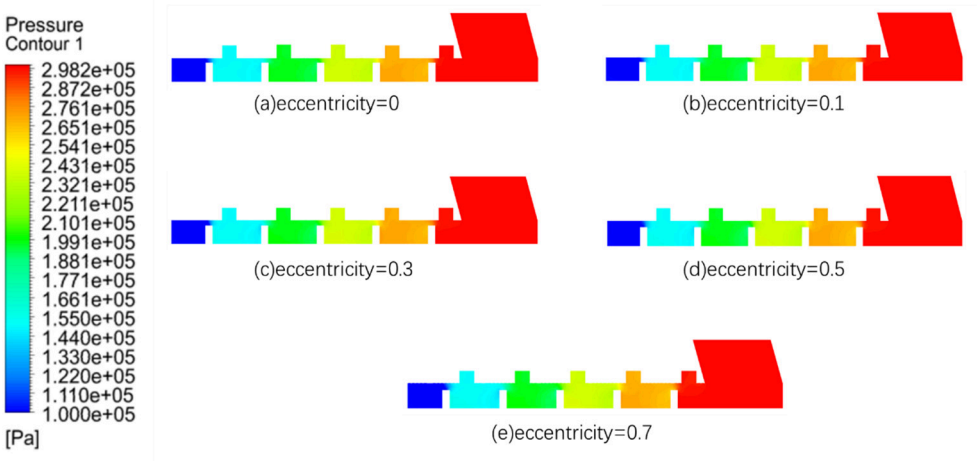

Figure 16. Pressure contour map of the gap flow field under different eccentricities.

From the analysis of the fluid mechanics mechanism, when the eccentricity increases, the gap on the biased side decreases, resulting in an increase in flow resistance and a limitation on the conversion of pressure energy to kinetic energy; the gap on the deviated side increases, leading to a decrease in flow resistance, but a wide gap is prone to form local circulation. Some gases that did not participate in axial leakage instead flow in the opposite direction, counteracting the improvement in the conversion efficiency of pressure energy. The combined effect of these two factors significantly suppresses the overall change in pressure loss rate, ultimately presenting a pressure distribution pattern that is asymmetric and with a stable loss rate [27]. To further reveal the asymmetric flow mechanism caused by rotor eccentricity, the circumferential pressure distribution of the sealing gap is presented in Figure 17. It can be clearly observed that the pressure exhibits an obvious non-uniform distribution along the circumferential direction. The pressure is relatively high on the narrow gap side where the rotor is biased, while it is significantly low on the wide gap side. This distinct circumferential pressure difference directly reflects the asymmetric throttling and flow resistance effects induced by eccentricity, which is consistent with the above analysis of pressure distribution and flow mechanism.

3.4.2. The Influence of Eccentricity on the Velocity Distribution of the Gap Flow Field

Figure 18 clearly presents the velocity distribution contour plots within the sealing gap of the air bearing under different eccentricities. When the eccentricity is 0, the axial velocity within the sealing gap is symmetrically distributed, and the high-speed areas are uniformly distributed along the sealing inlet section. As the eccentricity gradually increases to 0.7, the distribution pattern of the axial velocity changes synchronously with the asymmetry of the gap: the axial velocity peak on the side where the rotor leans towards increases, and the extension range of the high-speed area along the path shortens; the axial velocity peak on the side where the rotor deviates decreases, and the high-speed area shrinks towards the outlet side; the gradient of the axial velocity distribution significantly increases with the increase in eccentricity.

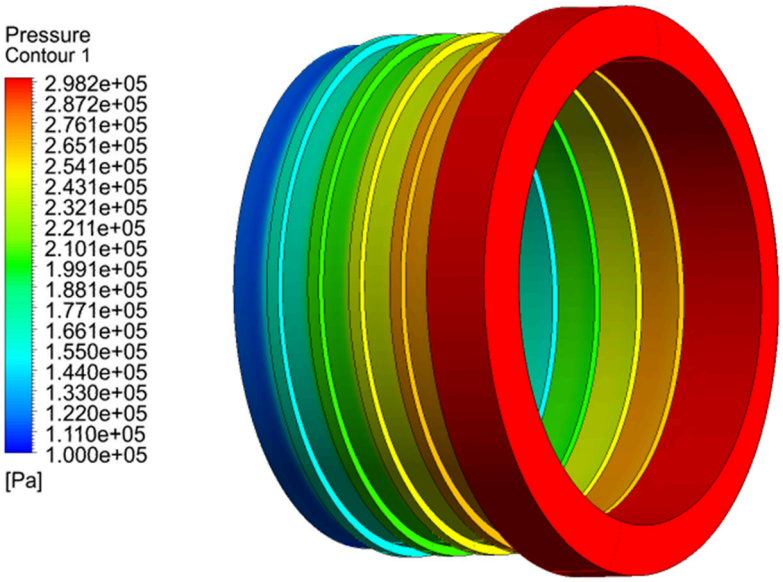

Figure 17. Circumferential pressure distribution of the sealing gap.

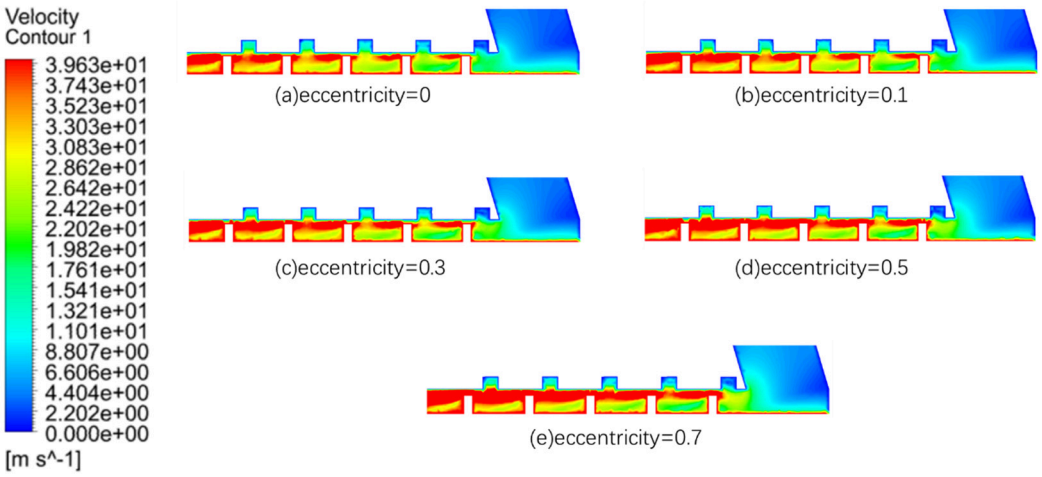

Figure 18. Axial velocity contour map of the gap flow field under different eccentricities.

The increase in eccentricity has a relatively small impact on the local backflow phenomenon at the sealing inlet. When the eccentricity is 0, the backflow area is symmetrically distributed, with an axial length of approximately 0.2 mm; when the eccentricity is 0.7, the backflow area shifts towards the off-center side, and the axial length only expands to 0.22 mm. The peak backflow velocity remains at around 15 m/s, further verifying that the eccentricity has a relatively weak overall influence on the axial flow field [28].

3.4.3. The Influence of Eccentricity on the Leakage of Hybrid Aerostatic/Aerodynamic Bearings

Table 5 presents the calculation results of the leakage volume of the hybrid aerostatic bearing seal under different eccentricities. Figure 19 shows the graph of the leakage volume of the hybrid aerostatic bearing seal varying with the eccentricity.

Table 5. Calculation Results of Gap Leakage Volume under Different Eccentricity Rates.

Gap Height (mm)	Inlet Pressure (MPa)	Rotor Speed (r/min)	Eccentricity	Gap Leakage Rate (kg/s)
0.10	0.3	60,000	0	0.00199
			0.1	0.00203
			0.3	0.00201
			0.5	0.00198
			0.7	0.00197

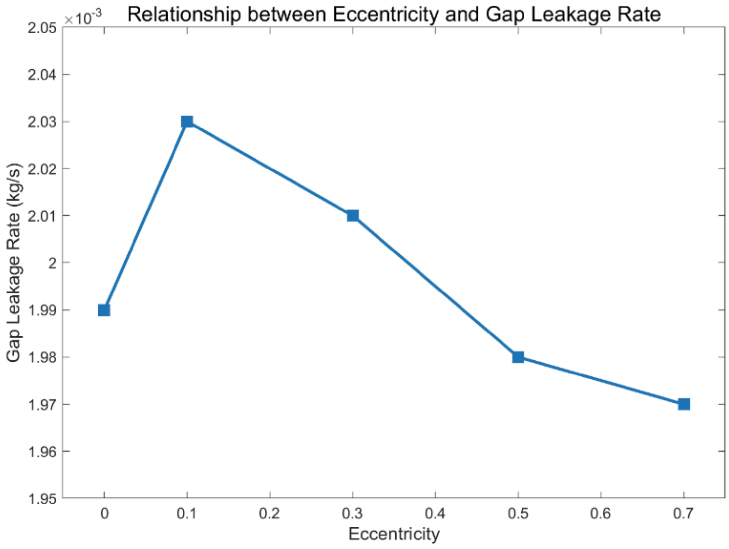

Figure 19. Graph showing the variation in clearance leakage quantity with eccentricity.

From Table 5 and Figure 19 it can be seen that, when the rotor eccentricity is relatively small, the gap leakage increases as the eccentricity increases. However, when the eccentricity is greater than 0.1, the gap leakage decreases as the eccentricity increases. Eccentricity has a negligible effect on leakage compared with clearance height and inlet pressure [29]. This is because, when the eccentricity is between 0 and 0.1, the eccentricity is small and the expansion of the flow area of the wide gap on the deviated side is greater than the reduction on the biased side. At this time, the backflow effect in the wide gap is weak and no obvious reverse flow is formed. The total effective flow area slightly increases, resulting in a slight increase in leakage [30]. When the eccentricity is between 0.1 and 0.7, as the eccentricity increases, the throttling effect of the narrow gap on the biased side continues to strengthen and the flow area further decreases. At the same time, the backflow effect in the wide gap on the deviated side is significantly enhanced and some axial flow gas is counteracted by the backflow, limiting the growth of the effective leakage flow and even causing a slight decrease. The reason why eccentricity has little effect on leakage is that the hydrodynamic effect induced by rotation is much smaller than the pressure-driven sealing flow effect. Eventually, the total leakage gradually returns to the baseline value [31].

4. Conclusions

This study takes the conical straight-tooth annular clearance sealed hybrid aerostatic/aerodynamic bearing as the research object. Based on steady compressible gas flow theory and CFD numerical simulation, the leakage characteristics and flow field evolution laws of four key parameters (clearance height, inlet pressure, rotor speed, and eccentricity) are systematically revealed. The main conclusions are as follows:

(1) The leakage rate shows significant sensitivity to structural and operating parameters. The leakage volume is nonlinearly and positively correlated with clearance height

and inlet pressure, following a power-law or polynomial relationship, and these two parameters dominate the leakage characteristics. The effects of rotor speed and eccentricity on leakage are both less than 5%, belonging to secondary influencing factors.

(2) The flow mechanism can be summarized as follows: increasing the gap height expands the hydraulic diameter, reduces flow resistance, and strengthens inlet vortex disturbance, thus increasing leakage. Increasing inlet pressure enhances the pressure potential energy driving force and intensifies local flow separation, which also promotes leakage. Rotor speed mainly diverts axial kinetic energy through circumferential shear, while eccentricity suppresses leakage variation through the coupling effect of biased-side throttling and deviation-side backflow, both showing weak effects on leakage.

(3) For engineering applications, the radial clearance is recommended to be controlled within 0.03–0.06 mm and the inlet pressure within 0.3–0.6 MPa. When eccentricity ≤ 0.5 and rotational speed $\leq 120{,}000$ r/min, the leakage fluctuation is within 2%, which can meet the stability requirements of high-speed turbomachinery.

Author Contributions: F.W.: conceptualization, methodology, software, validation, data curation, writing—original draft preparation, and formal analysis; Y.W.: investigation, resources, writing—review and editing, supervision, and project administration. All authors have read and agreed to the published version of the manuscript.

Funding: This research received no external funding.

Data Availability Statement: The raw data supporting the conclusions of this article will be made available by the authors upon request.

Conflicts of Interest: The authors declare no conflicts of interest.

References

1. Wang, X. Research on the Dynamic Characteristics and Structural Optimization of Typical Seals in Turbomachinery. Ph.D. Thesis, Shenyang Aerospace University, Shenyang, China, 2022.
2. Xu, W. Theoretical and Experimental Research on the Efficiency Enhancement and Vibration Reduction Performance of Adaptive Gas Film Seal for Turbomachinery. Ph.D. Thesis, Southeast University, Nanjing, China, 2018.
3. Wu, Y.; Gao, Y.; Zhou, S.; Li, X.; Zhang, H.; Chen, L.; Wang, Q.; Liu, J.; Sun, R.; Zhao, M.; et al. Experimental Study on the Characteristics of Typical Toothed Sealing of Gas Turbine Engine. *Turbine Technol.* **2024**, *66*, 275–278.
4. Wang, X. Analysis of Sealing Dynamic Characteristics and Research on New Sealing Anti-Vibration Mechanism. Ph.D. Thesis, Shenyang Aerospace University, Shenyang, China, 2019.
5. Chen, Y.; Huo, D.; Wang, G.; Li, X.; Zhang, H.; Liu, J.; Sun, R.; Zhao, M.; Wu, Q.; Zhou, L.; et al. Modelling and performance improvement of an annular grooved thrust air bearing. *Ind. Lubr. Tribol.* **2023**, *75*, 1116–1124. [CrossRef]
6. Song, L.; Yuan, G.; Zhang, H.; Li, X.; Chen, Y.; Wang, Q.; Liu, J.; Sun, R.; Zhao, M.; Zhou, L.; et al. The stability of spiral-grooved air journal bearings in ultrahigh speeds. *Materials* **2022**, *15*, 1759. [CrossRef]
7. Morosi, S.; Santos, I.F. Experimental investigations of active air bearings. In Proceedings of the Turbo Expo: Power for Land, Sea, and Air, Copenhagen, Denmark, 11–15 June 2011; pp. 901–910.
8. Radil, K.; Zeszotek, M. An experimental investigation into the temperature profile of a compliant foil air bearing. *Tribol. Trans.* **2004**, *47*, 470–479. [CrossRef]
9. Yue, Y.; Su, X.; Li, Z.; Wang, Q.; Liu, J.; Sun, R.; Zhao, M.; Zhou, L.; Chen, Y.; Zhang, H.; et al. Design and Parameter Optimization of Frictionless Cylinder Based on Air Bearing. *Opt. Precis. Eng.* **2022**, *30*, 678–688. [CrossRef]
10. Han, D.; Yang, J.; Zhao, C.; Li, X.; Zhang, H.; Liu, J.; Sun, R.; Wang, Q.; Zhou, L.; Chen, Y.; et al. Experimental Study on Vibration Characteristics of Hybrid aerostatic bearing-Rotor System. *J. Vib. Eng.* **2012**, *25*, 680–685.
11. San Andrés, L.; Delgado, A.; Yang, J. *Annular Clearance Gas Seals: Models and Measurements for Leakage, Force Coefficients and Their Effect on Rotor Stability*; Turbomachinery Laboratory, Texas A&M Engineering Experiment Station: College Station, TX, USA, 2022.
12. Sun, D.; Wang, S.; Ai, Y.; Li, X.; Zhang, H.; Liu, J.; Sun, R.; Wang, Q.; Zhou, L.; Chen, Y.; et al. Numerical Study on Static and Dynamic Characteristics of Negative Misalignment Seals. *J. Aerosp. Power* **2017**, *32*, 791–799.
13. Sun, D.; Xiao, Z.; Wang, X.; Li, X.; Zhang, H.; Liu, J.; Sun, R.; Wang, Q.; Zhou, L.; Chen, Y.; et al. Research on the Flow Characteristics of Negative Misalignment Sealing. *Proc. CSEE* **2015**, *35*, 3068–3074.

14. Hirano, T.; Guo, Z.; Kirk, R.G. Application of computational fluid dynamics analysis for rotating machinery—Part II: Labyrinth seal analysis. *J. Eng. Gas Turbines Power* **2005**, *127*, 820–826. [CrossRef]
15. Li, Z.; Li, Z.; Li, J.; Li, X.; Zhang, H.; Liu, J.; Sun, R.; Wang, Q.; Zhou, L.; Chen, Y.; et al. Leakage and rotordynamic characteristics for three types of annular gas seals operating in supercritical CO2 turbomachinery. *J. Eng. Gas Turbines Power* **2021**, *143*, 101002. [CrossRef]
16. Li, P.; Cao, L. Effect of rotor-stator axial gap on the tip seal leakage flow of a steam turbine. *J. Therm. Sci.* **2021**, *30*, 973–982. [CrossRef]
17. Kulkarni, D.; Mare, L. Development of a New Loss Model for Turbomachinery Labyrinth Seals. *J. Eng. Gas Turbines Power* **2023**, *145*, 061016. [CrossRef]
18. Elsayed, A.M.; Owis, F.M.; Abdel Rahman, M.M. Film cooling optimization using numerical computation of the compressible viscous flow equations and simplex algorithm. *Int. J. Aerosp. Eng.* **2013**, *2013*, 859465. [CrossRef]
19. Sajadmanesh, S.M.; Mohseni, A.; Mojaddam, M. Vortex dynamics mechanisms of separated boundary layer in a highly loaded low pressure turbine cascade. *Int. J. Heat Fluid Flow* **2020**, *82*, 108540. [CrossRef]
20. Zhang, E.; Watanabe, T.; Himeno, T.; Li, X.; Zhang, H.; Liu, J.; Sun, R.; Wang, Q.; Zhou, L.; Chen, Y.; et al. Leakage reduction mechanism of supercritical CO2 scallop damper seal: Vortex structure and turbulence dissipation. *Phys. Fluids* **2023**, *35*, 056108. [CrossRef]
21. Song, Y.; Li, M.; Zeng, F.; Li, X.; Zhang, H.; Liu, J.; Sun, R.; Wang, Q.; Zhou, L.; Chen, Y.; et al. The interaction mechanism between sealing flow and endwall secondary flow in the low-pressure vane of counter-rotating turbine. *Phys. Fluids* **2025**, *37*, 046123. [CrossRef]
22. Zhang, Z.; Zhang, Y.; Zhang, Y. Flow mechanism between purge flow and mainstream in different turbine rim seal configurations. *Chin. J. Aeronaut.* **2020**, *33*, 2162–2175. [CrossRef]
23. Wu, H.; Zhang, D.; Shen, X.; Li, X.; Zhang, H.; Liu, J.; Sun, R.; Wang, Q.; Zhou, L.; Chen, Y.; et al. Study on the suppression of tip leakage vortex in axial flow pumps based on circumferential grooving in the rotor chamber. *J. Mar. Sci. Eng.* **2025**, *13*, 972. [CrossRef]
24. Xue, H.; Zhang, J.; Chen, Y.; Li, X.; Zhang, H.; Liu, J.; Sun, R.; Wang, Q.; Zhou, L.; Chen, Y.; et al. Flow Mechanisms and Rotordynamic Characteristics of a Diaphragm Labyrinth Seal with Circumferential Micro-Nozzles. *Tribol. Int.* **2026**, *219*, 111888. [CrossRef]
25. Li, W.; Pu, W.; Ji, L.; Liu, M.; Yang, Q.; He, X.; Agarwal, R. Vortex dynamics characteristics in the tip region based on Wray–Agarwal model. *Phys. Fluids* **2024**, *36*, 013337. [CrossRef]
26. Lin, Q.; Li, Q.; Xu, P.; Li, X.; Zhang, H.; Liu, J.; Sun, R.; Wang, Q.; Zhou, L.; Chen, Y.; et al. Transport Mechanism and Optimization Design of LBM–LES Coupling-Based Two-Phase Flow in Static Mixers. *Processes* **2025**, *13*, 1666. [CrossRef]
27. Xing, Y.; Zhai, F.; Li, S.; Li, X.; Zhang, H.; Liu, J.; Sun, R.; Wang, Q.; Zhou, L.; Chen, Y.; et al. A study on radial oil seal leakage failure due to viscoelasticity under dynamic eccentricity. *Ind. Lubr. Tribol.* **2024**, *76*, 1197–1204. [CrossRef]
28. Vannini, G.; Mazzali, C.; Underbakke, H. Rotordynamic computational and experimental characterization of a convergent honeycomb seal tested with negative preswirl, high pressure with static eccentricity and angular misalignment. *J. Eng. Gas Turbines Power* **2017**, *139*, 052502. [CrossRef]
29. Li, Z.; Li, J.; Feng, Z. Numerical investigation on the leakage and static stability characteristics of pocket damper seals at high eccentricity ratios. In Proceedings of the Turbo Expo: Power for Land, Sea, and Air, Charlotte, NC, USA, 26–30 June 2017.
30. Wei, X.; Yao, Z.; Jin, F.; Li, X.; Zhang, H.; Liu, J.; Sun, R.; Wang, Q.; Zhou, L.; Chen, Y.; et al. Numerical simulation of flow and heat transfer characteristic in straight-through labyrinth seals of aeroengines under eccentric and rotating conditions. *J. Mech. Sci. Technol.* **2023**, *37*, 3173–3183. [CrossRef]
31. Chen, D.; Chen, S.; Tang, C.; Li, X.; Zhang, H.; Liu, J.; Sun, R.; Wang, Q.; Zhou, L.; Chen, Y.; et al. Effect of active compensation on the performance of self-eccentric lip seals: Numerical and experimental investigation. *Tribol. Int.* **2026**, *219*, 111852. [CrossRef]

Disclaimer/Publisher's Note: The statements, opinions and data contained in all publications are solely those of the individual author(s) and contributor(s) and not of MDPI and/or the editor(s). MDPI and/or the editor(s) disclaim responsibility for any injury to people or property resulting from any ideas, methods, instructions or products referred to in the content.